

Ferromagnetic resonance in a thin film of Heusler alloy Co₂FeSi

Author: Josep Rius Vázquez

Facultat de Física, Universitat de Barcelona, Diagonal 645, 08028 Barcelona, Spain.

Advisor: Joan Manel Hernández Ferràs

Abstract: Heusler alloys are promising ferromagnets to develop next generation digital memories and other electronic devices, with Co₂FeSi being one of the most interesting. This report describes the measurement of several magnetic properties of a thin film of this alloy, such as saturation magnetization, anisotropy field and Gilbert damping parameter, using the Ferromagnetic Resonance (FMR) technique.

I. INTRODUCTION

Digital technology is based on the processing of binary information by switching devices, like MOSFET or bipolar transistors, connected in a circuit. The binary data ('0' and '1') are materialized by the presence or absence of electrical charge stored in the circuit capacitances. Alternatively, the *spintronics* approach consists in using the intrinsic feature of the electron spin to have two possible values to replace the charge-based digital technology by a spin-based digital technology in the implementation of processing and storage functions. The latter presents certain advantages over the former, such as greater integration density, better processing speed, non-volatility or less power consumption [1].

Heusler alloys are promising materials for spintronic devices [2], such as spin transistors, magnetic RAMs or reading heads for hard disks, because of their good magnetoresistance characteristics. Among Co-based Heusler alloys, Co₂FeSi have attracted much interest due to its small Gilbert damping parameter and its compatibility with conventional fabrication processes in the semiconductor-based microelectronics industry [3].

The main technique to study the magnetic properties of such materials is Ferromagnetic Resonance (FMR). This technique consists to expose the samples to a static magnetic field \vec{B} . Under the action of this field, the elementary magnetic moments of the material (spins) start to oscillate, precessing around the axis defined by \vec{B} with the so called Larmor frequency $f_L = (\gamma/2\pi)B$, where γ is a constant (gyromagnetic ratio) coupling the angular and magnetic moments of the oscillating spin. Unavoidable damping mechanisms extract energy from the oscillation and reduce the precession amplitude with time. Therefore, after a short time, the spins become aligned parallel to the external applied field and the magnetization of the material is completed. However, if a time periodic small magnetic field perpendicular to \vec{B} is applied and its frequency coincides with the precession frequency (that is, at the resonant frequency), it supplies the energy lost due to damping and the spin precession remains indefinitely. In this way, by analyzing the energy absorbed by the material as a function of frequency and \vec{B} , it is possible to measure many of its magnetic characteristics. This is the

purpose of this report for the Heusler alloy Co₂FeSi.

It is divided in the following Sections: next Section is devoted to describe FMR with some detail. Section III shows the experimental setup and results, and Section IV discuss the findings of the work and extract conclusions.

II. FERROMAGNETIC RESONANCE

A. Free resonance

The magnetic moment $\vec{\mu}$ of a charged microscopic particle is related with its total angular momentum \vec{J} by the expression $\vec{\mu} = -g\mu_B\vec{J}$, where g is the Landé g -factor and μ_B is the Bohr magneton. If $\vec{\mu}$ is not aligned with an external field $\vec{B} = \mu_0\vec{H}$ (where μ_0 is the permeability of free space), a torque given by $\vec{T} = \vec{\mu} \times \vec{B}$ applies to the particle. Because of the coupling between magnetic moment, $\vec{\mu}$, and angular momentum, $\hbar\vec{J}$, the latter changes at a rate $\hbar d\vec{J}/dt = \vec{T}$. Then, by combining all these equations we obtain

$$\frac{d\vec{\mu}}{dt} = -\gamma\vec{\mu} \times \vec{B}, \quad \gamma = \frac{g\mu_B}{\hbar} \quad (1)$$

Now, by defining the magnetization vector, \vec{M} , as the magnetic moment per unit volume and using the relation $\vec{B} = \mu_0(\vec{H} + \vec{M})$, equation (1) can be written as

$$\frac{d\vec{M}}{dt} = -\gamma\mu_0\vec{M} \times \vec{H} \quad (2)$$

If \vec{M} does not have the same direction as \vec{H} , equation (2) shows that \vec{M} precesses about \vec{H} at a constant angle with a motion similar to that a gyroscope precessing under the influence of gravity. If $\vec{H} = (0, 0, H_z)$, then $\vec{M} = (m_x, m_y, m_z)$ where $m_x, m_y \ll m_z \approx |\vec{M}|$. The precession frequency is given by

$$f_0 = (\gamma/2\pi)\mu_0H \quad (3)$$

However, this free precession analysis neglects losses. In reality, magnetic damping is always present and the precession amplitude decreases with time. The magnetization falls in a spiral to the \vec{H} direction until it reaches

the equilibrium after a certain time period that depends on the material magnetic properties.

The previous analysis is valid for the so called uniform mode (with wavenumber $k = 0$) where all elementary moments inside the material are parallel and precess together in phase [4].

B. Driven and damped resonance

Consider now applying a small time harmonic in-plane magnetic field \vec{b} with frequency f , perpendicular to the static field $\vec{B} = \mu_0 \vec{H}$, with time dependence proportional to $\exp(-i2\pi ft)$ (see Fig. 1). If $\vec{B} = \mu_0(0, 0, H_z)$ and $\vec{b} = \mu_0(h_x, 0, 0)$, the transverse amplitudes of the resulting magnetization m_x, m_y , increase when the applied frequency f approximates the precession frequency f_0 . This increase is at the expense of the energy supplied by \vec{b} , thus indicating that some energy of this field is being absorbed by the material. In absence of damping, the absorption becomes infinite at $f = f_0$; that is, a strong resonant peak of absorption appears. In practice, the amplitude increase of m_x, m_y due to the field \vec{b} compensates for losses, and the resonant peak has a finite height when $f = f_0$.

The dynamics of the described process is well represented by the Landau-Lifshitz-Gilbert (LLG) equation:

$$\frac{d\vec{M}}{dt} = -\gamma\mu_0\vec{M} \times \vec{H}_{eff} + \frac{\alpha}{M}\vec{M} \times \frac{d\vec{M}}{dt} \quad (4)$$

where the first term on the right side is the same as equation (2), with \vec{H}_{eff} being the total effective field acting on the magnetization produced by all the spin interactions, and the second term being a phenomenological expression to consider a viscous damping controlled by the dimensionless Gilbert damping parameter α .

As said above, \vec{H}_{eff} is the sum of multiple interactions, like demagnetizing field or anisotropy field, in addition to the external applied field \vec{H} . Thus, equation (3) must be modified to take into account these extra interactions. For thin films and external field $\vec{B} = \mu_0(0, 0, H_z)$ parallel to the sample plane (see Fig. 1), it transforms into the following Kittel equation [4]:

$$f_0 = (\gamma/2\pi)\mu_0\sqrt{(H + H_k)(H + H_k + M)} \quad (5)$$

where $H = H_z$ is the external field and H_k and $M \approx M_s$ (M_s is the saturation magnetization of the material) are the contributions of the anisotropy and demagnetizing fields, respectively. If these contributions are negligible, equation (5) reduces to equation (3).

Additionally, parameter α is correlated with the half linewidth ΔB of the resonant peak according to the following expression [5]:

$$\Delta B = (4\pi\alpha/\gamma)f_0 + \Delta B_0 \quad (6)$$

where the frequency independent second term on the right side arises from the presence of magnetic inhomogeneities in the sample. This linear relationship between linewidth and resonant frequency is what is expected if only the viscous damping mechanism described by the LLG equation exists.

Equations (5) and (6) enable f_0 and α of a ferromagnetic material such as Co₂FeSi to be experimentally known.

If instead of being parallel, \vec{B} is perpendicular to the sample plane, then the Kittel equation (5) changes to

$$f_0 = (\gamma/2\pi)\mu_0(H - M) \quad (7)$$

where the linear dependence of f_0 on H is valid if $M \approx M_s$ [4].

III. EXPERIMENTAL SETUP AND RESULTS

A. Experimental FMR setup

To perform the FMR experiment it is necessary to control the intensity of the external static field \vec{B} , and the frequency f and intensity of the driven magnetic field \vec{b} . Fig. 1 shows a sketch of the required equipment.

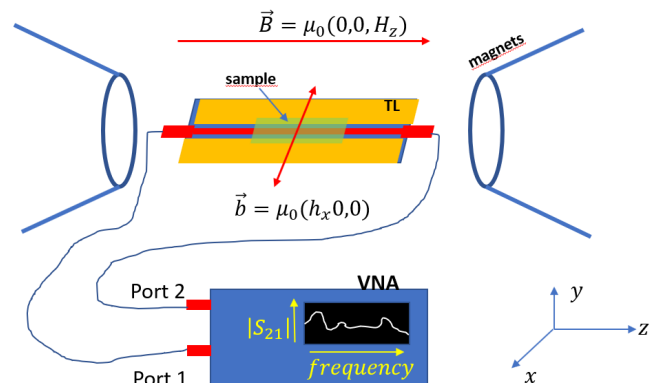


FIG. 1: Sketch of experimental setup. TL: transmission line, VNA: Vector Network Analyzer, $|S_{21}| =$ power received at port2 divided by power sent by port 1.

A 21 nm thick rectangular monocrystalline Co₂FeSi film (sample) grown on a GaAs substrate, is placed on top of a transmission line (TL) parallel to the xz plane. The sample is immersed in a static magnetic field $\vec{B} = \mu_0(0, 0, H_z)$ generated by an electromagnet. A power supply (not shown in Fig. 1) supplies the required current to electromagnet. Ports 1 and 2 of a Vector Network Analyzer (VNA) are connected to the left and right ends of the TL, respectively. The VNA supplies microwave power at a given frequency through port 1, $P_1(f)$, and receives the power arriving at port 2, $P_2(f)$. In this way the sample is also exposed to the small RF

magnetic field $\vec{b} = \mu_0(h_x, 0, 0)$ perpendicular to \vec{B} . Ratio $|S_{21}|(f) = |P_2(f)/P_1(f)|$ is measured by the VNA, normalized (and identified as ΔS_{21}) and registered. The power supply and the VNA itself are controlled by a PC through a LabView program to sweep B and frequency f in the desired ranges.

B. Results

In our experiments f is swept in two ranges: 0.1-15 GHz and 20.1-23 GHz. The field intensity of B is swept in the range ± 0.5 T and the \vec{b} power is fixed to 0 dBm.

The measurements were made with two orientations for the long edge of sample, i.e. parallel to the z axis (expressed as 0 degrees in this report) and at 45 degrees from this axis. Both orientations correspond to symmetry planes of the sample. Fig. 2 shows the results as a projection of ΔS_{21} (codified in color) on the B - f plane for sample orientations 0° (Fig. 2a) and 45° (Fig. 2b).

A third measurement was made by applying \vec{B} perpendicular to the sample plane (Fig. 2c). In this case, the B intensity is swept from 1.0 to 1.8 T and f was in the range 1-15 GHz.

C. Extracting the field at resonance, B_0

The following step involved extracting the value of the field at resonance, B_0 , at each of the about 180 frequencies of the graphs in Fig. 2 from the raw results. This was achieved by writing a MATLAB script that fits ΔS_{21} vs. B with an analytic function (a Lorentzian plus its derivative) at each frequency, as shown in red lines in the example insets of Fig. 2. From the fitting, it is possible to find the field of the resonant peak, B_0 , at each frequency. The results are shown in Fig. 3 for both sample orientations, 0° , 45° , and for \vec{B} perpendicular to the sample plane.

The good agreement between equation (5) (dashed lines in Fig. 3) and the experimental points, which allow the anisotropy field $\mu_0 H_k$ and saturation magnetization $\mu_0 M_s$ values of the sample to be calculated. These values are shown in Table I.

	$\mu_0 H_k$ [mT]	$\mu_0 M_s$ [T]
0°	5.6 ± 0.4	1.49 ± 0.01
45°	3.96 ± 0.06	1.457 ± 0.001

TABLE I: Co_2FeSi anisotropy field and saturation magnetization for 0° and 45° sample orientations.

For the case of \vec{B} perpendicular to the sample plane, B_0 values are given in Fig. 3c, and Table II shows the $\mu_0 H_k$ and $\mu_0 M_s$ fitted values extracted from the fitting line of Fig. 3c in the high frequency range ($f > 9$ GHz), where $M \approx M_s$.

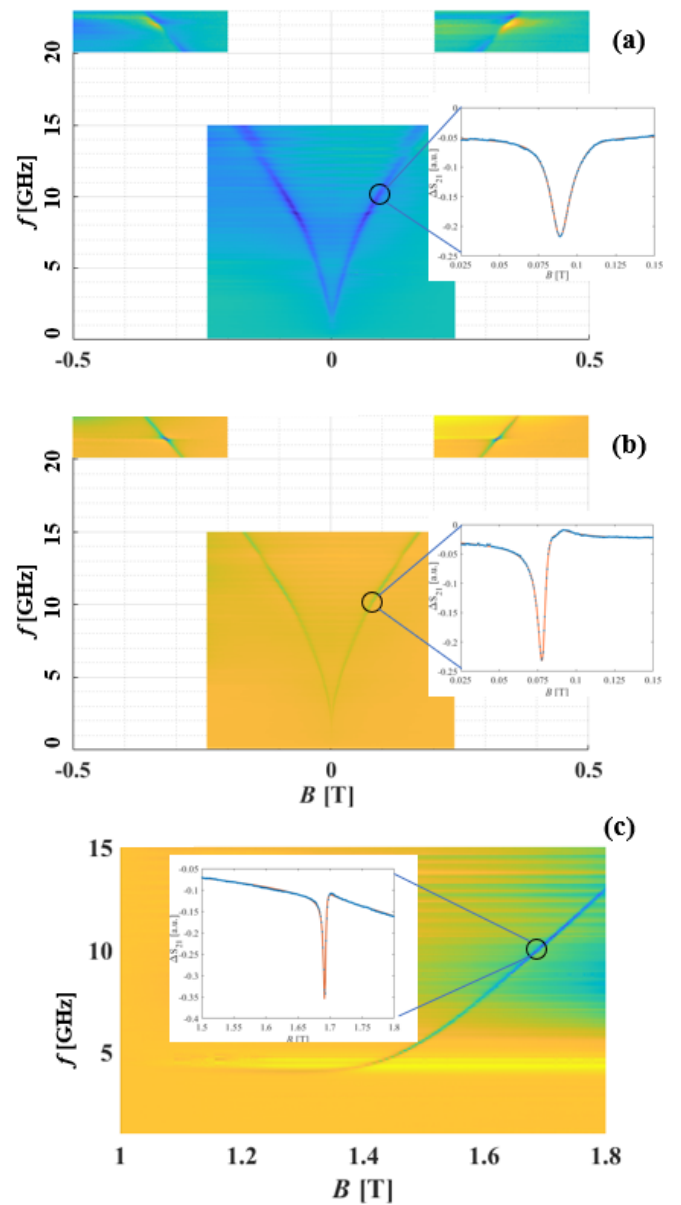


FIG. 2: Lines of FMR for sample orientation at (a): 0° , (b): 45° (see text), and (c): \vec{B} perpendicular to sample plane. Insets show examples of absorption peak profiles at 10 GHz (in blue, experimental points, in red, fitting line).

$\mu_0 H_k$ [mT]	$\mu_0 M_s$ [T]
139.7 ± 0.4	1.48 ± 0.02

TABLE II: Anisotropy field and saturation magnetization for \vec{B} perpendicular to the sample plane.

As can be seen in Fig. 3a, for 0° , two very close resonance peaks not present at the 45° orientation appear for f in the range of 13 to 15 GHz. This can be the result of inhomogeneities of the RF field \vec{b} inside the sample exciting non-uniform modes of precession with wavenumbers $k > 0$ [6], [9].

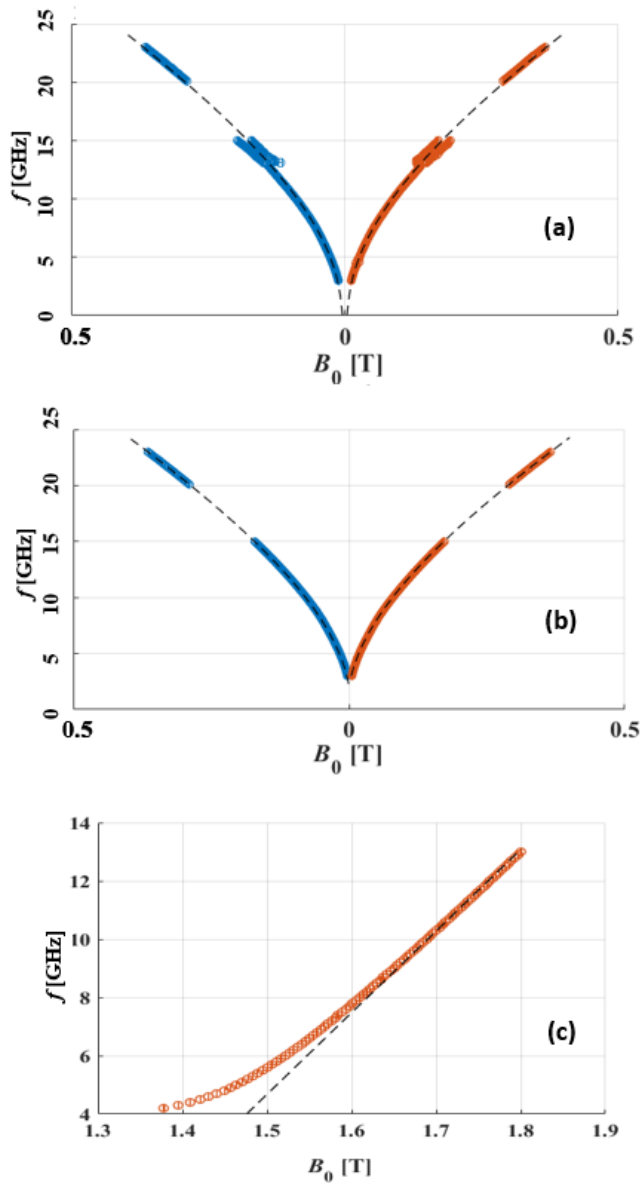


FIG. 3: Fields and frequencies of resonance peaks for sample orientations 0° , (a), 45° , (b) and field \vec{B} perpendicular to the sample, (c). The error bars are too small to be seen at this scale. Dashed lines are obtained by fitting from equation (5) and (7).

D. Extracting line width ΔB at resonance

The fitting of S_{21} as a function of B also enables linewidth ΔB of the resonant peak to be determined as a function of frequency f in order to verify the accuracy of equation (6), and calculate α as the slope of a straight line. Fig. 4 shows the 0° results when f ranges from 3 to 13 GHz and 20 to 23 GHz with positive B . For 45° , the responses for positive and negative fields are superimposed when f ranges from 3 to 15 GHz and 20 to 23 GHz.

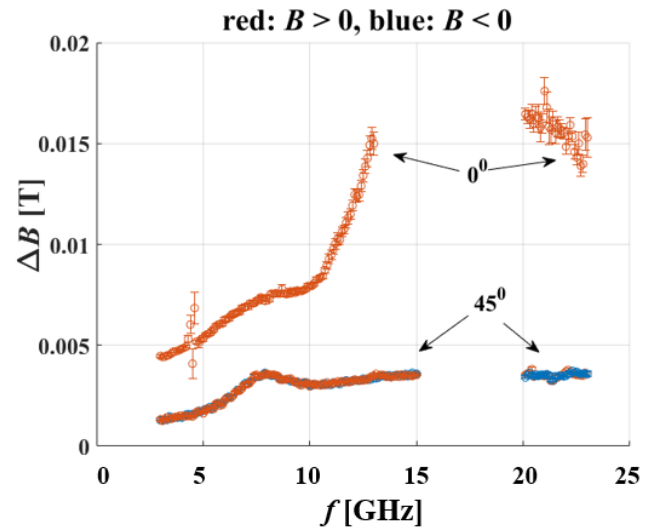


FIG. 4: Line width for sample orientation 0° and 45° as a function of frequency. For 0° only is shown the case $B > 0$.

As mentioned above, if the only existing damping mechanism is that represented by the second term of LLG equation, a linear dependence of ΔB on frequency (equation (6)) is expected. Figure 4 shows that this is not the case. There clearly exists an additional damping mechanism. A possible explanation is described in [7] and [8]. According to the authors, the additional damping mechanism is due to two-magnon scattering caused by lattice defects or dislocations. As a consequence, they propose a modified equation (6) as

$$\Delta B = (4\pi\alpha/\gamma)f_0 + \Delta B_0 + \Delta B_{0TMS} \quad (8)$$

where the first two terms represents the normal Gilbert damping (equation (6)) and ΔB_{0TMS} is due to the two-magnon scattering.

For the perpendicular to the sample \vec{B} case, normal Gilbert damping is observed in the range of frequencies where the frequency has a linear dependence on field (approximately from 9 GHz to 13 GHz in Fig. 3c), and the values of ΔB_0 and α can be determined from equation (6). The results are shown in Table III and Fig. 5.

α	ΔB_0 [mT]
$(1.3 \pm 0.9) \times 10^{-3}$	1.4 ± 0.7

TABLE III: Gilbert damping parameter and remaining field for perpendicular to the sample \vec{B} .

IV. CONCLUSIONS

FMR experiments were performed to extract magnetic characteristics (resonant field, anisotropy, damping parameter) of the Heusler alloy Co_2FeSi at its three symmetry axis, by applying an external static field in [1 0

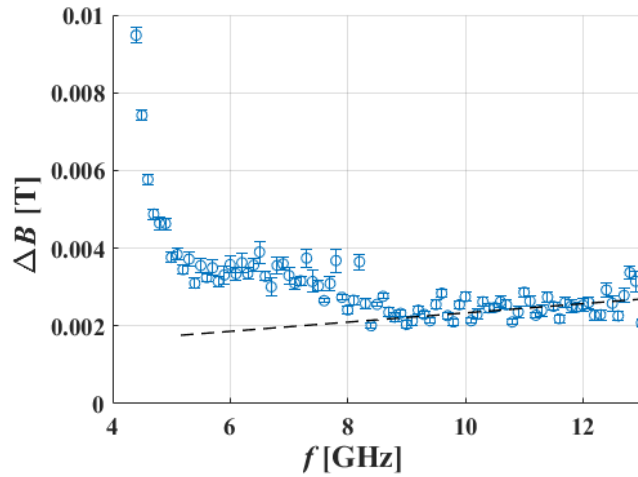


FIG. 5: Line width for \vec{B} perpendicular to the sample as a function of frequency. Dashed line is obtained by fitting from equation (6).

0] (0°) and [1 1 0] (45°) in-plane directions and the out-of-plane [0 0 1] (perpendicular) direction, and a small transverse RF magnetic field. Postprocessing of raw results showed a good agreement of the field at resonance, B_0 , with theory (Fig. 3a, b and c), in all cases. Additionally, anisotropy field and magnetization saturation

(Tables I and II), and the damping parameter α for the perpendicular to the sample field case (Table III), are found.

A significant difference on how the linewidth of the resonance peak depends on frequency was found when: a) \vec{B} was parallel to the sample plane (Fig. 4), where equation (6) fails; and b) when \vec{B} was perpendicular to the sample plane (Fig. 5), where equation (6) is satisfied. This dissimilarity is attributed to the presence of two-magnon scattering as an additional damping mechanism in the sample in-plane orientations [7], [8].

In the 0° sample orientation, a double resonant peak was observed in one range of the external field, which is attributed [6], [9] to the presence of an additional mode of precession with $k > 0$, in addition to the uniform mode analyzed in this report.

Acknowledgments

I would like to thank to Joan Manel Hernández, my advisor, for his help and guidance over the development of the TFG. I am also thankful to Marc Rovirola for providing the perpendicular to the sample raw data and sharing his knowledge during our discussions in the lab. Last but not least, I am extremely grateful to Dolors for her patience and support over the years.

[1] P. Rey and J.N. Roy, *Spintronics. Fundamentals and Applications*, (Springer, Singapore 2021).
 [2] K. Elphick, W. Frost, M. Samiepour, T. Kubata, K. Takanashi, H. Sukegawa, S. Mitani and A. Hirohata, "Heusler alloys for spintronic devices: review on recent development and future perspectives", *Science and Technology of Advanced Materials*, Vol. 22, No. 1, pp. 235-271 (2021).
 [3] K. Srinivas, T. Prasanna Kumari, M. Manivel Raja, et al., "Effect of Fe substitution for Co on structure, electrical resistivity, and magnetic properties of Heusler type $\text{Co}_{2-x}\text{Fe}_{1+x}\text{Si}$ alloys", *J. Appl. Phys.* 114, 033911 (2013).
 [4] Ch. Kittel, *Introduction to Solid State Physics*, (John-Wiley & Sons, New York 2005, 8th. ed.).
 [5] L. Lu, "Damping mechanisms in magnetic recording materials and microwave assisted magnetization reversal", PhD

Dissertation, Colorado State University, (2014)
 [6] S.M. Rezende, *Fundamentals of Magnonics*, (Springer, Heidelberg 2020)
 [7] S. Mizukami, D. Watanabe, M. Oogane, Y. Ando, Y. Miura, M. Shirai and T. Miyakazi, "Low damping constant for Co_2FeAl Heusler alloy films and its correlation with density of states", *J. Appl. Phys.* 105, 07D306 (2009)
 [8] W.K. Peria, T.A. Peterson, A.P. McFadden, T. Qu, C. Liu, C.J. Palmstrom and P.A. Crowell, "Interplay of large two-magnon ferromagnetic resonance linewidths and low Gilbert damping in Heusler thin films", *Phys. Rev. B*, 101, 134430 (2020)
 [9] S. Chikazumi, *Physics of Ferromagnetism*, (Oxford University Press, New York 1997).